doi:10.1016/j.jmb.2005.01.060 J. Mol. Biol. (2005) xx, 1–16

JMB

Available online at www.sciencedirect.com

SCIENCE DIRECT®

ELSEVIER

Nucleotide Dependent Motion and Mechanism of Action of p97/VCP

Byron DeLaBarre and Axel T. Brunger*

Howard Hughes Medical Institute, and Departments of Molecular and Cellular Physiology, Neurology and Neurological Sciences, and Stanford Synchrotron Radiation Laboratory, Stanford University J.H. Clark Center E300-C 318 Campus Drive, Stanford CA 94305-5432, USA

*Corresponding author

The AAA (ATPases associated with a variety of cellular activities) family of proteins bind, hydrolyze, and release ATP to effect conformational changes, assembly, or disassembly upon their binding partners and substrate molecules. One of the members of this family, the hexameric p97/valosin-containing protein p97/VCP, is essential for the dislocation of misfolded membrane proteins from the endoplasmic reticulum. Here, we observe large motions and dynamic changes of p97/VCP as it proceeds through the ATP hydrolysis cycle. The analysis is based on crystal structures of four representative ATP hydrolysis states: APO, AMP-PNP, hydrolysis transition state ADP·AlF_3, and ADP bound. Two of the structures presented herein, ADP and AMP-PNP bound, are new structures, and the ADP·AlF_3 structure was re-refined to higher resolution. The largest motions occur at two stages during the hydrolysis cycle: after, but not upon, nucleotide binding and then following nucleotide release. The motions occur primarily in the D2 domain, the D1 α-helical domain, and the N-terminal domain, relative to the relatively stationary and invariant D1α/β domain. In addition to the motions, we observed a transition from a rigid state to a flexible state upon loss of the γ-phosphate group, and a further increase in flexibility within the D2 domains upon nucleotide release. The domains within each protomer of the hexameric p97/VCP deviate from strict 6-fold symmetry, with the more flexible ADP state exhibiting greater asymmetry compared to the relatively rigid ADP·AlF_3 state, suggesting a mechanism of action in which hydrolysis and conformational changes move about the hexamer in a processive fashion.

Keywords: AAA (ATPases associated with a variety of cellular activities) protein; membrane protein extraction; endoplasmic reticulum-associated degradation

Introduction

Mammalian valosin-containing protein p97/VCP[1] is a 540 kDa hexameric protein found in all tissue types. It has close homologs in fly,[2] yeast,[3] plant,[4] and protozoa.[5] p97/VCP is essential for endoplasmic reticulum-associated degradation (ERAD).[6–8] p97/VCP is required to move membrane-bound proteins from the endoplasmic reticulum (ER) into the cytosol in an ATP-dependent manner, a process referred to as protein dislocation. Protein dislocation is necessary for subsequent proteasomal degradation of misfolded ER proteins. When ERAD is defective or overwhelmed, the accumulation of misfolded proteins in the ER results in stimulation of the unfolded protein response,[9] and can eventually cause cell-death. Apart from its role in removing misfolded proteins from the ER, p97/VCP regulates cellular pathways by degradation of proteins, such as NF-KB[10,11] and the transcription factor SPT23.[12] p97/VCP interacts with numerous adaptor proteins such as p47, Ufd1 and Npl4.[13,14] While some of these adapter proteins have been implicated directly in ERAD,[15] others have been shown to direct p97/VCP to a role in altering membrane morphology.[14,16] A membrane protein complex in the ER membrane has been identified that is involved in retrograde

Abbreviations used: VCP, valosin-containing protein; ER, endoplasmic reticulum; ERAD, endoplasmic reticulum-associated degradation; AAA, ATPases associated with a variety of cellular activities; MAD, multi-wavelength anomalous dispersion.

E-mail address of the corresponding author: brunger@stanford.edu

membrane protein transport and that interacts with p97/VCP.[17,18]

The p97/VCP protomers are comprised of three major domains joined by conserved linkers. Each protomer consists of an N-terminal domain followed by tandem repeats (D1 and D2) of ATPases associated with a variety of cellular activities (AAA) domains. The N domains are structurally similar to the N domains of other proteins with tandem AAA repeats (NSF, Sec18p, VAT),[19–23] despite low levels of sequence identity and different cellular functions.[24] The D1 and D2 AAA domains are a combination of two smaller domains: an α/β domain and an α domain. There is a moderate degree of homology (41% sequence identity and 72% sequence similarity) between the two AAA domains of p97/VCP, with most of the conserved residues in the α/β domains. Nucleotides bind in a region between the α and the α/β domains, but interact primarily with their respective α/β domain. A pronounced conserved feature of AAA domains is the sensor-2 motif.[25] This motif is comprised of conserved arginine or lysine residues that have been shown in other AAA protein family members to interact with nucleotides in adjacent protomers.[21,26] Mutation of these residues in several different AAA proteins have been shown to affect ATP hydrolysis.[27,28]

Here, we present two new crystal structures of p97/VCP with ADP and AMP-PNP (referred to simply as ATP) bound to the D2 domain, respectively. We present a re-refinement of the structure of p97/VCP with the transition state mimic ADP·AlF_3 (referred to simply as ATP‡) at somewhat higher resolution. Diffraction resolution was limited in all structures, but this was overcome by collection of experimental multi-wavelength anomalous dispersion (MAD) diffraction data and frequent use of cross-validation *via* the free *R* value in order to reduce the risk of overfitting when trying diffraction data cutoffs and refinement schemes. All crystal structures have ADP bound to the D1 nucleotide-binding site, so they are referred to by the occupant of the nucleotide-binding site in the D2 domain. The ATP, ATP‡, and ADP structures, along with the APO state,[29] comprise representative states that encompass the nucleotide hydrolysis cycle. Accordingly, we present an analysis of the

Table 1. ATP, ATP‡, and ADP diffraction data

Data set	Space group	Unit cell parameters *a*, *b*, *c* (Å) α, β, γ (deg.)	λ (Å)	Resn (Å)	Total/ unique reflections	% Complete (last shell)	R_{merge}[a] (%) (last shell)	$I/\sigma I$ (last shell)
ATP								
Native	*P*3	*a*=144.9, *b*=144.9, *c*=164.4, α=β=90, γ=120	1.0316	23–3.1	295293/ 60820	85 (27)	11.7 (72.1)	8.8 (1.0)
Native[b]	*P*3	*a*=144.9, *b*=144.9, *c*=164.4, α=β=90, γ=120	1.0316	23–3.5	262233/ 48496	99.6 (100)	11.2 (51.8)	10.5 (2.2)
Semet Peak	*P*3	*a*=145.5, *b*=145.5, *c*=164.5, α=β=90, γ=120	0.9792	46–4.5	176002/ 23064	99.3 (100)	8.7 (18.2)	11.8 (4.7)
ATP‡								
Native	*I*222	*a*=162.64, *b*=178.02, *c*=321.14, α=β=γ=90	0.9791	29.9–4.4	174589/ 28110	91 (53.5)	10.3 (70.5)	10.1 (0.8)
ADP								
Semet (peak A)	*I*222	*a*=163.96, *b*=178.40, *c*=320.53, α=β=γ=90	0.9788	30.0–4.25	326438/ 33219	99.3 (99.6)	7.6 (35.3)	13.4 (2.1)
Semet (peak B)	*I*222	*a*=162.62, *b*=178.18, *c*=316.45, α=β=γ=90	0.9798	44.3–6.0	106627/ 11792	99.6 (100)	5.6 (45.6)	13.4 (1.2)
Semet (inflection B)	*I*222		0.9801	44.5–6.0	53229/11783	99.5 (100.0)	5.6 (37.5)	11.6 (1.6)
Semet (remote B)	*I*222		0.9611	43.3–6.0	53072/11759	99.4 (100.0)	6.0 (38.3)	10.6 (1.5)

[a] $R_{merge} = \sum_{hkl} \sum_i |I_i(hkl) - I(hkl)| / \sum_{hkl} \sum_i I_i(hkl)$.

[b] Since the native ATP diffraction data (first row) were anisotropic (ranging from approximately 3.5–3.1 Å resolution), the diffraction data were re-processed to 3.5 Å. This data set was used for refinement.

conformational and dynamic changes of p97/VCP that occur during nucleotide hydrolysis.

p97/VCP undergoes motions primarily at two stages of the nucleotide hydrolysis cycle: between the ATP and ATP‡ states, and between the ADP and APO states. Three regions undergo order–disorder transitions during the hydrolysis cycle: the D2α domain, the D1D2 linker region, and the sensor-2 region of the D2 domain. Nucleotide-induced domain motions from the D2 domain are transmitted *via* the D1D2 linker region to the D1α domain. The D1α domain makes multiple contacts with the N domain and serves to regulate the motion of the N domain.

Results

The overall structure of p97/VCP in the ATP‡ state has been discussed.[30] Here, we present new structures of p97/VCP in two other nucleotide states, ATP and ADP, at higher resolution (Tables 1 and 2). We assume that the nucleotide analog AMP-PNP and the transition-state mimic ADP + AlF_x are similar to, if not identical with, the ATP and transition states, respectively, of the molecule. All structures discussed here were crystallized as complete hexamers, corresponding to the biologically relevant unit of p97/VCP. Both the ATP‡ and ADP structures contained three protomers in the asymmetric unit such that the hexamer is generated by a crystallographic 2-fold symmetry operator. The three protomers exhibited rigid-body conformational variability as discussed in further detail below. The p97/VCP·ATP (AMP-PNP) complex crystallized with four protomers in the asymmetric unit, such that two complete hexamers are generated from crystallographic 3-fold symmetry operators. There was essentially no variation among the four independent protomers. The APO state of p97/VCP crystallized with a single protomer in the asymmetric unit; a 6-fold crystallographic operator completes the hexamer for this crystal form.[29]

The phase-combined and *B* sharpened electron density maps for the various structures solved in our laboratory (i.e. ATP, ATP‡, and ADP) provided sufficient detail to analyze the motion of rigid bodies and secondary structural elements, but precluded a detailed high-resolution analysis of the atomic contacts accompanying the domain motions. There are some exceptions to this limitation: the quality of the electron density maps was sufficient for the identification of several key residues interacting with nucleotides in both the D1 and D2 domains, as well as for allowing a detailed view of the interactions between the N and D1 domains. While the interface between N and D1 domains was described in a previously published p97/VCP structure lacking the D2 domains,[31] here we observed these interactions within the context of a full-length molecule in multiple nucleotide states. We found that despite the lower-resolution limit of the crystallographic data for the ADP and ATP‡ structures (4.25 Å and 4.4 Å, respectively), the electron density for the D2α domain is clearly visible in both the ADP and ATP‡ states, while it is disordered for the ATP and APO structures at 3.5 Å

Table 2. Refinement statistics

Structure	ATP	ATP‡	ADP
Resolution range	30–3.5	30–4.4	30–4.25
R_{work} (%)[a]	30.6	26.8	27.2
R_{free} (%)[b]	32.7	33.9	33.9
Number of reflections			
For refinement	91,879	22,707	51,285
For R_{free} calculation	4798	1607	4091
Total number of atoms in refinement	21,888	16,617	16,732
Bulk solvent probe/shrink (Å)	1.25/0.75	2.5/2.5	1.0/1.0
Bulk solvent level ($e^-/Å^3$)	0.109	0.164	0.124
Bulk solvent *B*-factor ($Å^2$)	26.9	371	83.2
Δ_{bonds}	0.0099	0.009	0.013
Δ_{angles}	1.7	1.72	2.49
Average *B*-factor all atoms($Å^2$)	34.4	280	241.92
Cross-validated σ_A coordinate error (Å) (8–3.5 Å)	0.99	1.35	2.07
NCS r.m.s.d. relative to the A chain			
B chain	0.002	1.12	0.270
C chain	0.004	1.44	0.270
D chain	0.005/0.020	–	–
Ramachandran analysis (for all residues)[c]			
Most favored region (%)	53.7	42.4	46
Allowed region (%)	40	45.1	42.9
Generously allowed region (%)	5.6	12.3	10.7
Disallowed region (%)	0.7	0.2	0.4

[a] $R_{work} = \sum_{hkl}(|F_o| - k|F_c|)/\sum_{hkl}|F_o|$ for reflections not in R_{free} set.
[b] R_{free} is computed from a random 7.5% selection of reflections in the asymmetric unit that was not used during refinement.
[c] As defined by the criteria of Procheck.[53]

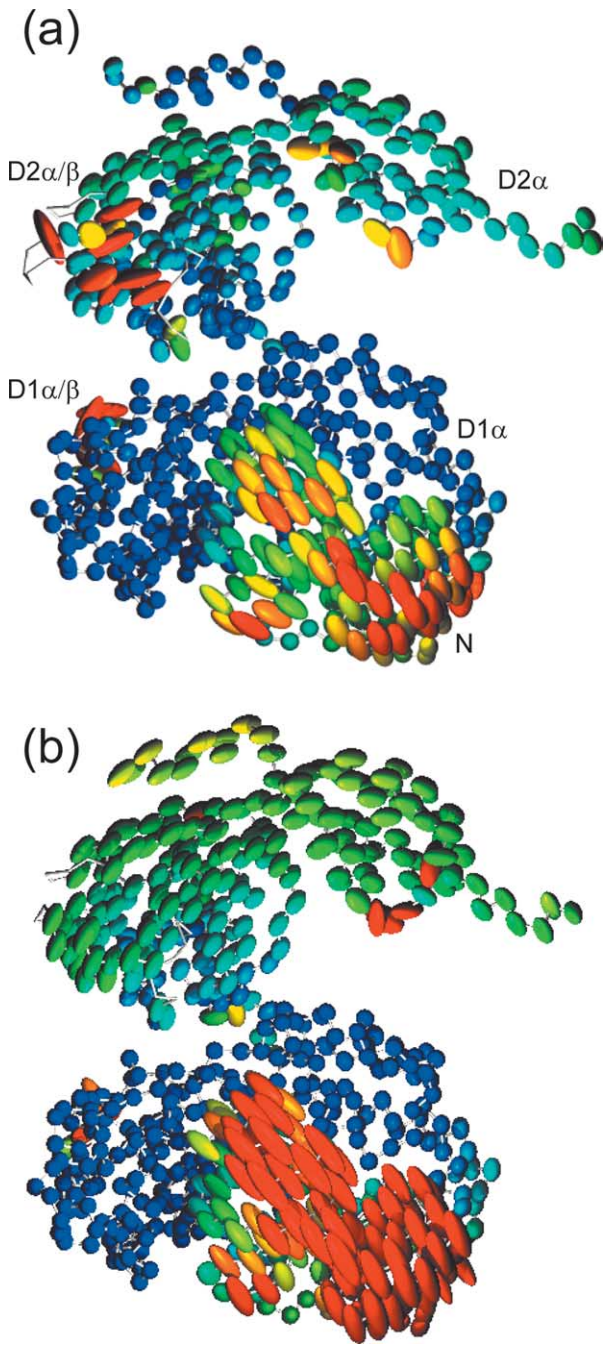

Figure 1. Conformational variability; deviation from 6-fold symmetry. Conformational differences between the three independent protomers in the asymmetric unit are shown for the (a) ATP‡ and (b) ADP crystal structures. The same view was used for both panels. Pseudo-ellipsoids were generated as described in Materials and Methods. The color scale (blue to red) indicates the magnitude of the deviation from 6-fold symmetry (0.5–5.0 Å). Ellipsoids that are pointing in a similar direction indicate groups of residues that are moving as rigid bodies.

and 3.6 Å resolution, respectively. Thus, overall resolution is not necessarily correlated with quality of electron density maps throughout the model.

Deviations from 6-fold symmetry: interprotomer conformational variability

The presence of multiple protomers within the asymmetric units of the individual crystal structures was used to assess the conformational variability of p97/VCP for the ATP‡ and ADP nucleotide states. This was not possible for the APO state,[29] since the entire hexamer is generated from a single protomer by crystallographic symmetry. For the ATP state, the four protomers in the asymmetric unit were identical except for minor differences in the ordering of the final visible residues in the C terminus (residues 730–735) at a crystal contact. Conformational variability of the APO and ATP states was probably affected by crystal packing and/or affected by the high ionic strength of the crystallization conditions used for these states.

The ATP‡ and ADP states crystallize in the same space group in low ionic strength conditions with three independent protomers, so a comparison of the conformational variability is meaningful. There is significantly more variability for the ADP state compared to the ATP‡ state (Figure 1; Tables 3 and 4). For the ADP state, the N domain of the C protomer is rotated by 6.8° and the N domain of the B protomer is rotated by 3.8°, with respect to the N domain in the A protomer. The conformational differences are similar to those observed between nucleotide states (discussed below). The conformational differences within the D2 domains of the ADP structure and all domains within the ATP‡ structure are relatively small, of the order of 1–2°. The large range of motions observed for the N domains in the ADP states provides a potential explanation for the absence of the N domains in the cryo-electron microscopy (cryo-EM) reconstructions of p97/VCP in this state.[32] It is likely that the N domains move over an even larger range under the conditions used for cryo-EM, as the molecules would not be restrained by the crystal lattice as they were for the X-ray analysis.

Nucleotide-dependent conformational changes

Several lines of evidence suggest that the D1 domain is catalytically inactive, despite the fact that the nucleotide-binding site contains all residues necessary for ATP hydrolysis. First, all structures of p97/VCP presented here and those solved previously show the unambiguous presence of ADP in all D1 domains, despite different crystal forms and the presence of other nucleotides in the crystallization conditions.[29–31] Second, the fully formed hexamer can exchange only six of the 12 sites

Table 3. Deviations from 6-fold symmetry for the N domains in the ATP‡ state (values in degrees)

	B	C
A	1	1.7
B	–	0.7

Table 4. Deviations from 6-fold symmetry for the N domains in the ADP state (values in degrees)

	B	C
A	3.8	6.8
B	–	3.6

available for nucleotide binding *in vitro*,[30] and there are only two or three sites active at any one time during ATP hydrolysis.[33] Third, the presence of, but not hydrolysis of, the D1 nucleotide is required for efficient assembly of the hexamer.[34,35] However, *in vitro* ATPase assays of p97/VCP seem to indicate an effect on ATPase activity for mutations in both the D1 and D2 nucleotide-binding domains.[15] Also, the D1 domain exhibits some ATPase activity at non-physiological temperatures (50–60 °C).[36] It remains to be seen if the D1 domain undergoes hydrolysis *in vivo* in the context of co-factors, substrates and proximity to the ER membrane surface.

Since the D1 domain is invariant in all observed crystal structures, we can analyze only nucleotide-dependent changes induced by the D2 domain. In the ATP and ADP structures, each of the four protomers in the asymmetric unit is occupied by AMP-PNP and ADP, respectively, in the D2 nucleotide-binding site. In the ATP‡ crystal structure, the D2 domains are occupied by a mixture of ADP and ADP·AlF_3. In the initial refinement at lower resolution,[30] we assumed identical occupancy in all of the D2 nucleotide-binding sites. However, upon extension of the diffraction data to higher resolution, the electron density maps revealed somewhat different occupancy for the AlF_3 moiety for each of the D2 nucleotide-binding sites in the three protomers of the asymmetric unit (not shown). Of the three protomers (A, B, and C, respectively), only the C protomer has unambiguous density for the presence of ADP·AlF_3. The B protomer indicates a state of partial occupancy for the AlF_3 moiety in addition to a fully occupied ADP molecule. The electron density for the nucleotide species in the A protomer shows electron density for ADP only.

Electron density for all domains and secondary structural elements is sufficient to characterize the motions of p97/VCP during the hydrolysis cycle (Figures 2 and 3 and Table 5). The D1α/β domain shows the least amount of motion during the hydrolysis cycle. It comprises the inner core of the p97/VCP hexamer and it is in a central location, connecting to all other domains. It shows the least deviation from 6-fold symmetry (Figure 1). We propose that the D1α/β domain comprises a fulcrum or structural base for motion of other domains in p97/VCP. For this reason, changes of the other domains are described with reference to the D1α/β domain.

The D2α domain undergoes order–disorder transitions during the hydrolysis cycle. Much of the domain is clearly visible in the ATP‡ and ADP structures but it is mostly disordered in both the

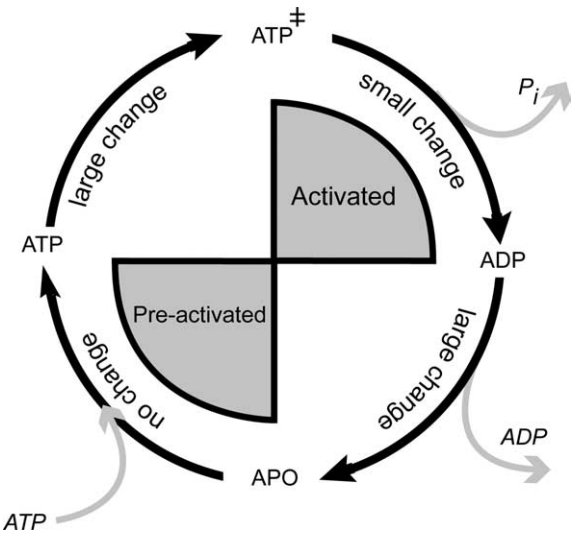

Figure 2. Conformational and dynamic changes during the hydrolysis cycle. Summary of the conformational and dynamic changes observed in the four representative nucleotide states APO, ATP, ATP‡, and ADP. The largest conformational changes occur between the pre-activated (APO and ATP) and activated (ATP‡ and ADP) states. The ATP‡ transition state is the most rigid structure, showing the least disorder and less asymmetry than the ADP state. The APO and ATP states are the states with the least amount of order in the D2 domains.

APO and ATP structures. The four other domains (N, D1α/β, D1α, and D2α/β) exhibit largely rigid-body motions that are described by translation and rotation operators. With an average value of less than 3 Å during the hydrolysis cycle, the translational operators are relatively small, considering the estimated coordinate error of the crystal structures (Table 2). Therefore, domain motions were approximated as simple rotations about axes running through the center of mass of a particular domain.

Large and opposing changes in domain orientation were observed at two points within the nucleotide hydrolysis cycle: between the ATP and the ATP‡ states, and between the ADP and the APO states (Figures 2 and 3). The conformational changes between the four structures can thus be described approximately as a conformational switch between two principal groups of states, one comprised of the APO and ATP states, and the other comprised of the ATP‡ and ADP states. These two groups are referred to as the pre-activated and the activated states, respectively, within the nucleotide cycle. Remarkably, the changes in domain orientation between the pre-activated and activated states are essentially mirror images of one another. The only significant deviation from this simplified two-state description is the motion of the D2α/β domain. There is a rotation of the D2α/β domain during the ATP‡ to ADP transition about an axis that is different from the axes of rotation observed for the other interstate changes.

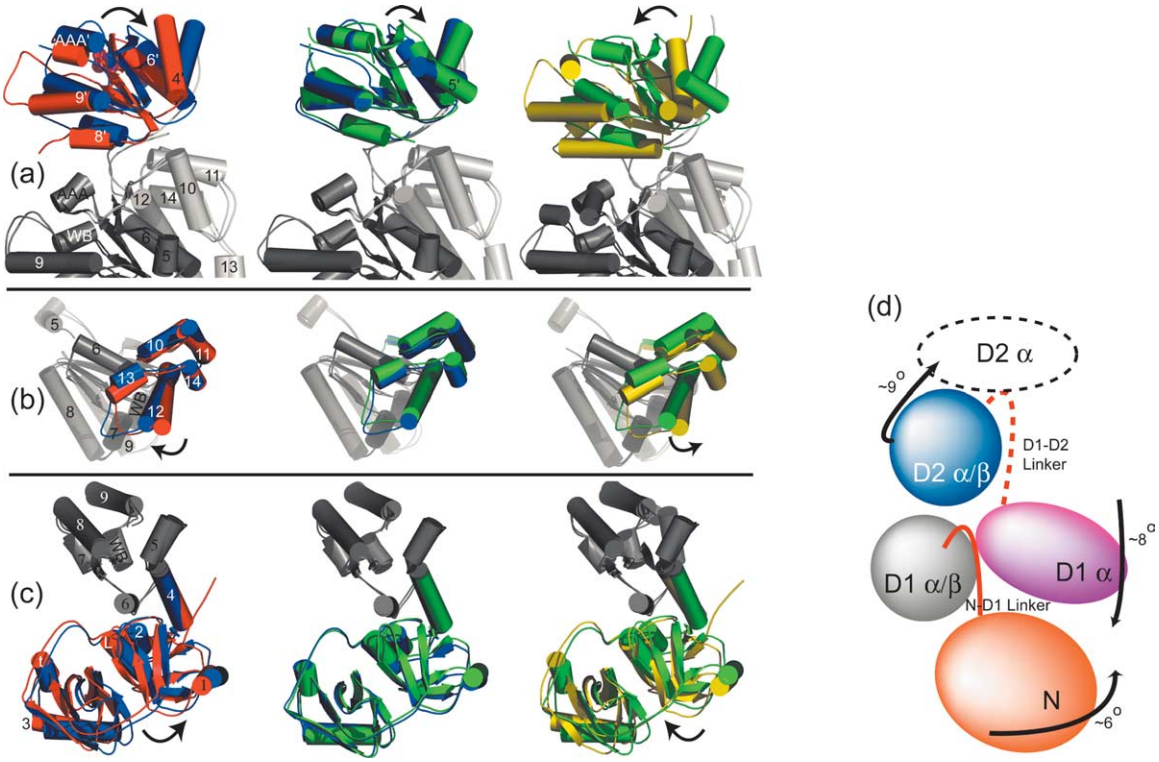

Figure 3. Nucleotide-dependent domain motions. Motions for the (a) D2α/β, (b) D1α, and (c) N domains are displayed between pairs of the ATP (red), ATP‡ (blue), ADP (green), and APO (yellow) state structures. Adjacent domains for the principle domain shown in (a), (b) or (c) are shown, in gray, for reference. The superposition of the APO and ATP structures showed minimal differences and is therefore not depicted here. The orientations of the views are the same for each transition. The views were chosen such that the axis of rotation for a particular domain motion is perpendicular to the plane of the page, with the exception of the ATP‡ to ADP (blue to green) transition, for which the view has been oriented such that the rotation axis is ∼45° off the perpendicular toward the right-hand side of the page. Arrows indicate the direction of the motions. Helices are numbered according to the p97/VCP numbering scheme (WB, Walker B helix; L, linker helix).[30] (d) A simplified diagram summarizing the domain motions from the ATP to the ATP‡ state. The N-D1 linker is shown in solid color, the D2α domain and D1D2 linker are shown with broken lines. The D2α domain and the D1D2 linker become ordered in the transition from the ATP to the ATP‡ state. All motions are described relative to the invariant D1α/β domain.

The motion between the activated and pre-activated states of p97/VCP is accompanied by two order–disorder transitions within the molecule, in addition to the above-mentioned order–disorder transitions of the D2α domain. These transitions occur within the D2 sensor-2 motif, and in the linker joining the D1 and D2 domains. Because all structures presented here are derived from diffraction data of similar quality, the observed order–disorder transitions can be interpreted as differences in stabilizing interactions for the particular structural elements or domains.

The sensor-2 motif contains a lysine or arginine residue that is thought to serve as a means of interprotomer communication in multimeric AAA proteins. In the D2 domain of p97/VCP, the sensor-2 motif is ordered in the pre-activated state and disordered in the activated state (Figure 4). The orientation of the key arginine "finger" residue, Arg 638, as well as the nearby but slightly less conserved Arg635, is such that they are both pointing away from the neighboring nucleotide and into their own protomer (Figure 4(b)). This was unexpected, since the proposed role of the sensor-2 residues is to interact with the nucleotide of the neighboring protomer. In contrast, in the D1 domain of

Table 5. Nucleotide-dependent domain rotations (values in degrees)

Domain	ATP–ATP‡	ATP‡–ADP	ADP–APO	APO–ATP
D1α	7.9/6.0/5.3	1.9/2.5/3.2	6.5/4.0/4.1	1.3
D2 α/β	8.9/8.3/7.8	5/4.7/3.4	12.3/12.5/11.5	0.5
N	5.5/2.9/2.3	2.5/1.8/3.8	6.8/4.1/5.4	2

Values are $x/y/x$ for the A, B, and C protomers, respectively, for the pairwise nucleotide state differences, except for the difference between APO and ATP, which refers to only a single protomer. All rotations are described with reference to the D1α/β domain, residues 224–357, of protomer A for each of the nucleotide states. The domain rotation angles were determined with LSQMAN.[52]

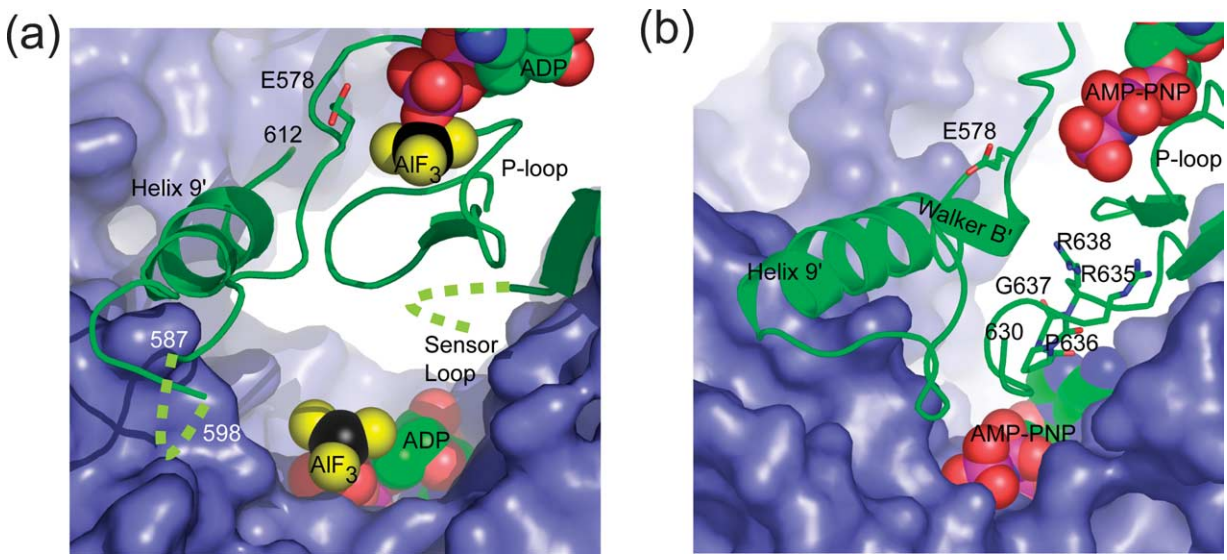

Figure 4. Conformational transition around D2 sensor-2. Nucleotide-dependent conformational changes of interprotomer interactions are shown for the (a) ATP‡ and (b) ATP structures around the sensor-2 loop in the D2 domain. Protomer A is represented as a green cartoon, the adjacent protomer B is represented by a blue surface, and the nucleotide atoms are represented by filled spheres. In the ATP‡ state, the disordered sensor-2 loop residues and the disordered loop between residues 587 and 598 are shown as broken green lines.

p97/VCP, the sensor-2 motif is ordered in all nucleotide states and it interacts with the neighboring protomer. The distance is 3.4 Å between D1 Arg 359 and the β-phosphate group of ADP in the neighboring protomer in the ATP state (Figure 5(a)). Similar interactions are observed in all other nucleotide states (data not shown).

The order–disorder transition in the D1D2 linker region affects residues 461 through 480 (Figure 5(b)–(d)). No electron density can be seen for residues 469 through 482 in the ATP state, whereas electron density is clearly visible for the all main-chain and several side-chain atoms of the linker for both activated states, i.e. ATP‡ ($ADP \cdot AlF_3$) and ADP. Thus, the D1D2 linker is ordered in the activated states and disordered in the pre-activated states.

Conformational changes in the D1 nucleotide-binding site

ADP interacts with the D1 nucleotide-binding site in two key areas (Figure 5(a)). There are interactions between the phosphate oxygen atoms and the backbone amide groups and the carbonyl groups of the P-loop residues that are invariant for all p97/VCP nucleotide states (as characterized by the occupancy of the D2 binding sites). Interestingly, another set of interactions varies slightly among the p97/VCP nucleotide states; these occur on opposite ends of the bound nucleotide. The first interaction is between the ribose 2′ hydroxyl group and His384 at the ribose end of the nucleotide, and the second interaction is between the ADP β-phosphate group and Lys251 at the diphosphate end of the nucleotide.

His384 is located on the C-terminal end of helix 10 within the D1α domain. In the ATP structure, the His384 N^{τ} and the nucleotide ribose 2′-OH are within hydrogen bonding distance of 2.9 Å (Figure 5(a)). This interaction remains intact for the ATP‡ transition state, but then lengthens upon hydrolysis in the ADP state; the distance increases from 2.7 Å in the ATP‡ C protomer to 4.6 Å in the ADP C protomer. Clear electron density for the entire Lys251 is visible only in the ATP structure. Based on the absence of electron density, the N^{ε} amino group of Lys251 does appear not to interact in a high-affinity manner with the β-phosphate group of the bound ADP molecule in other nucleotide states.

Conformational changes in the D2 nucleotide-binding site

The nucleotide environment in the D2 domain shows larger conformational changes compared to the D1 domain in accord with the ATPase activity of the D2 domain (Figure 5(b)–(d)). Significant conformational changes occur for three of the residues that interact with the bound nucleotide: Lys524, located in the Walker A motif; Lys658, located at the C-terminal end of helix 10′; and Asp478, located within the D1D2 linker. In the ATP state, all three of these residues are disordered or do not interact with the nucleotide (Figure 5(b)) in a high-affinity manner. In the C protomer of the ATP‡ state, Asp478 interacts with the ribose 2′-OH, Lys658 forms van der Waals interactions with the adenine ring, and Lys524 interacts both with the AlF_3 moiety that mimics the departing γ-phosphate group (Figure 5(c)). Lys524 interacts also with the carbonyl oxygen

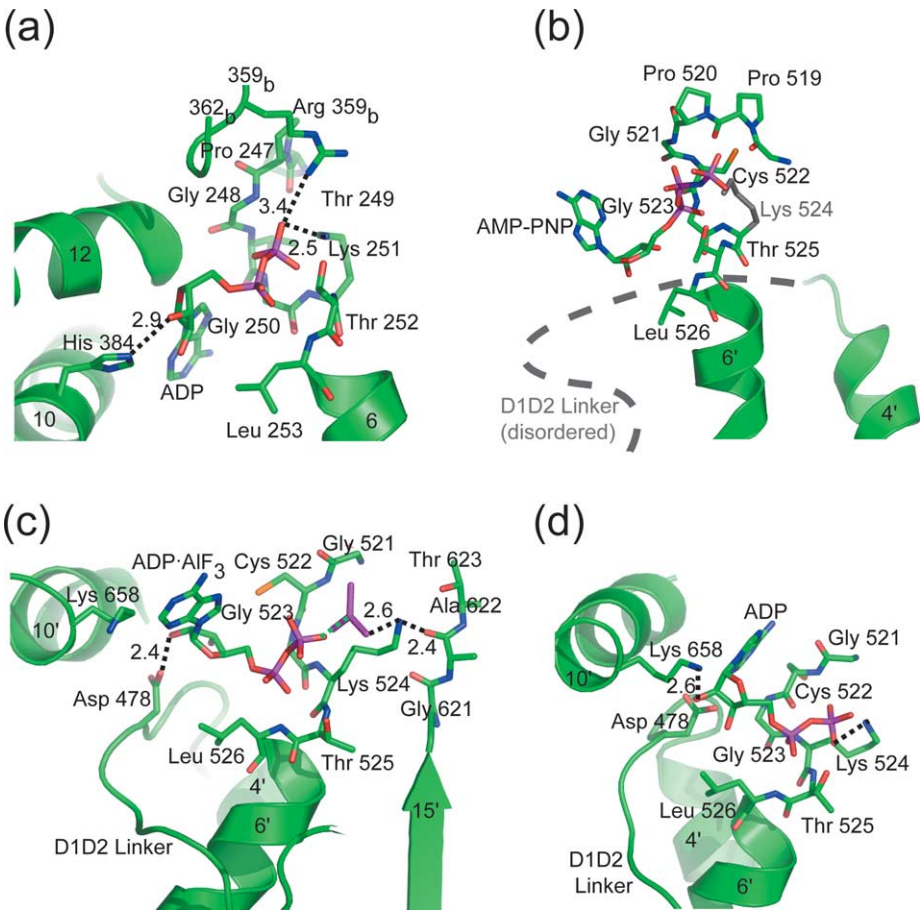

Figure 5. Nucleotide domain interactions. (a) Interactions of ADP with the D1 domain in the ATP structure. Note the interaction between the nucleotide and the D1 sensor-2 loop residue Arg359 from a neighboring protomer; neighboring residues are labeled with a subscript b. (b) Interactions of AMP-PNP with the D2 domain in the ATP structure. The disordered D1D2 linker is shown as a broken line and the disordered Lys524 is colored gray. (c) ATP‡ ($ADP \cdot AlF_3$) interactions in the D2 domain. (d) Interactions of ADP with the D2 domain in the ADP structure. In all cases, the A protomer is shown; the interactions are similar for the other protomers. Non-bonded distances that are less than 3.2 Å are shown as broken black lines; the values are in Å. Structural elements are represented as cartoons. ADP, the P-loop, and other interacting residues are represented as sticks.

atom of Ala622 in the loop following β-strand 15′. Thus, the nucleotide in the ATP‡ state interacts with three structural domains: the D2α/β domain (*via* β-strand 15′, the Walker A P-loop, and helix 6′), the D2α domain through helix 10′, and the D1D2 linker through Asp478. The tight interaction between the nucleotide and the domains results in an overall increased order within the D2 domain for this nucleotide state.

In the ADP state (Figure 5(d)), the interactions between the nucleotide molecule and residues Lys524, Asp478, and Lys658 shift slightly from what is observed in the ATP‡ state. Lys524 still interacts with the β-phosphate oxygen atom, but no longer interacts with the loop following β-strand 15′. The interaction between Asp478 and the ribose 2′-OH is replaced by an interaction between Lys658 and the 2′-OH. Apart from these variable interactions, there is an invariant series of interactions between the phosphate oxygen atoms and the P-loop residues of the D2 domain in all nucleotide states.

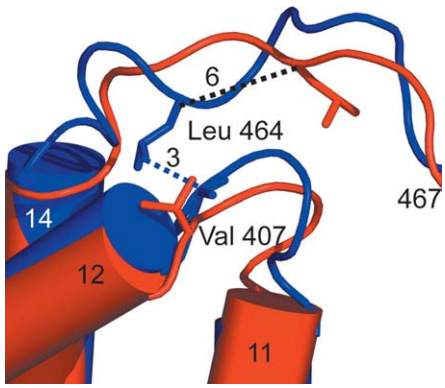

Figure 6. Conformational change of the D1α domain. The conformational change between the ATP (red) and ATP‡ (blue) states is shown for the loop between helices 11 and 12, and part of the D1D2 linker. Leu464 moves approximately 6 Å between the ATP and the ATP‡ states. In the ATP‡ state, Leu464 and Val407 are then only ∼3 Å apart. Note that the disorder in the D1D2 linker for the ATP state begins at residue 469, just beyond the region depicted here. All distances are shown in Å.

Conformational change of the D1α domain near the D1D2 linker

The primary contact between the D1D2 linker and the D1α domain occurs between residues 460 and 465 of the linker region and between residues 403 and 407 in the loop between D2α helices 11 and 12. The D1D2 linker moves with respect to the 11-12 loop in the transition from the pre-activated to the activated states, such that there is a change in the interaction between two hydrophobic residues. In the ATP state, Leu464 and Val407 are over 7.5 Å apart from one another, whereas in the ATP‡ state, Val407 is ~3 Å apart from Leu464 (Figure 6). This is a result of an approximately 6 Å shift in the position of the Leu464 C^{α} atom.

Interactions between the N and D1 domains

Electron density maps for the pre-activated ATP state were well defined for both the N and D1 domains (Figure 7(a) and (b)). The loop between helices 10 and 11 of the D2α domain intercalates itself into the loop between β strands 8 and 9 of the N domain. Asn387 mediates an interaction between Arg155 and the backbone carbonyl group of Arg159. Whereas other residues in the vicinity show side-chain density, there is essentially no electron density for the side-chain of Arg155 in the activated states (Figure 7(c)), suggesting that Arg155 has become disordered. This interaction is of particular interest, since mutations of Asn387 and/or Arg155 in human p97/VCP result in a Paget-related neuropathy (G. Watts, personal communication).[37]

Discussion

We determined the crystal structures of full-length p97/VCP in the ATP‡, AMP-PNP, and ADP states. The APO state has been solved,[29] along with truncated versions of p97/VCP lacking the D2 domain both alone[31] and in complex with a fragment of the adaptor protein p47.[38] All structures have ADP bound in the D1 nucleotide-binding site, while the occupant of the D2 nucleotide-binding site reflects the nucleotide crystallization condition.

On the basis of our analysis of the conformational changes between nucleotide states, the p97/VCP nucleotide states can be divided into two groups: those in the pre-activated state (APO and ATP), and those in the activated states (ATP‡ and ADP). A large conformational change occurs between the activated state and the pre-activated state and, conversely, an approximately opposite conformational change between the pre-activated state and the activated state. Several lines of evidence suggest that the p97/VCP hexamer does not undergo simultaneous hydrolysis in all six protomers; rather, that the hydrolysis occurs in a cooperative manner such that two protomers undergo hydrolysis at any one time.[36] Thus, ATP may occupy a D2 binding site and not undergo hydrolysis until other elements of the p97/VCP hexamer are aligned properly. The ATP structure was crystallized from a high ionic strength solution, a condition that has been shown to inhibit ATP hydrolysis by p97/VCP.[36] Thus, it is unlikely that equal occupancy by the non-hydrolyzable ATP analog AMP-PNP of all six D2 nucleotide-binding sites in the p97/VCP hexamer represents a physiologically relevant state of the p97/VCP hexamer. Nonetheless, the conformation of each single protomer occupied with a particular ATP analog should provide a close approximation to the conformation of the individual protomers *in vivo*.

The invariance of ADP in the D1 domain in all crystal structures suggests that during nucleotide hydrolysis, ATP is bound, hydrolyzed and released from the D2 domains only. Our analysis of the conformational changes during the hydrolysis cycle indicates that the ADP-bound D1α/β domain does not undergo any significant motion. Because of this immobility and its location within the central core of the hexamer, the D1 α/β domain is a fulcrum for motions of the other domains in the protein.

The conformational changes that accompany binding, hydrolysis, and release of the nucleotide must be transmitted from the D2 domain to the N domains. We proposed earlier that the conformational changes are transmitted through the D1D2 linker to the D1α domain,[30] and then onto the N domain. The presumed importance of the interaction between the D1α and N domain (Figure 7) is supported by the discovery of a human disease linked to the mutation of residues in the D1α/N interface.[37] With the work described here, we now have a detailed account of the motions that occur as p97/VCP progresses through the nucleotide hydrolysis cycle. The D1α domain rotates by ~8° with respect to the D1α/β domain. This alters its contacts with both the D1D2 linker and the N domain (Figure 3(b) and (d)), allowing it to regulate motion of the N domains. In this manner, conformational changes that start in a region near the C terminus of the protein are transmitted to the N terminus of the protein.

Several structural elements exhibit order–disorder transitions during the hydrolysis cycle (Figures 3(d), 4, and 5). One such element is the sensor-2 motif. In the transition from the pre-activated state to the activated state, the sensor-2 motif in the D2 domain of an adjacent protomer switches from an ordered conformation to a state in which it cannot be observed in the electron density maps. The Arg638 residue within the sensor-2 motif is the best conserved among similar AAA proteins within this motif,[39] and would be capable of interacting with the negatively charged departing γ-phosphate group after ATP hydrolysis has occurred. However, the interactions observed in the ATP‡ state indicate that the role of stabilizing the negative charge of a departing γ-phosphate group during ATP hydrolysis is fulfilled by Lys524. The

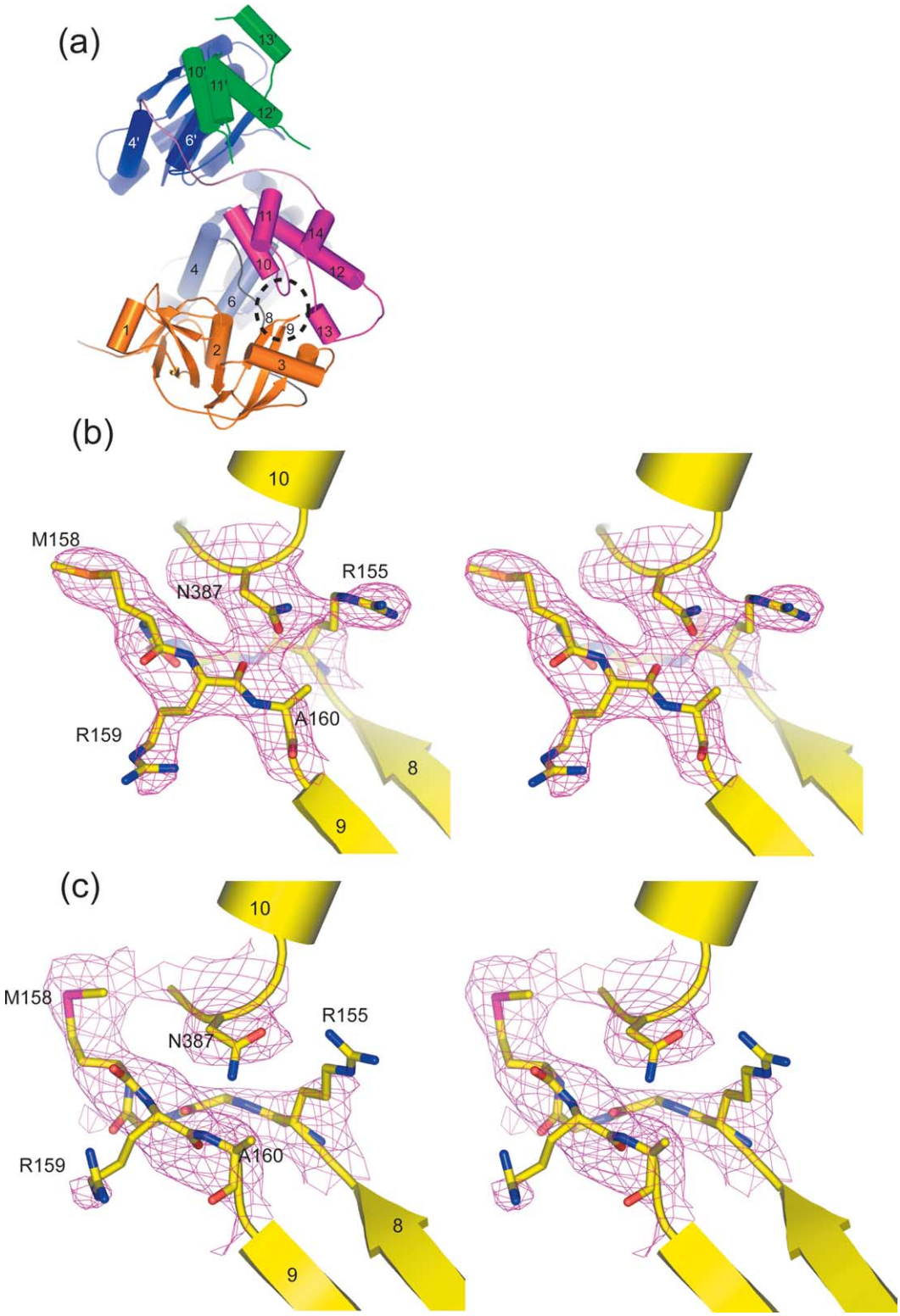

Figure 7. Interaction between the N and D1 domains. (a) The interaction between the D1α and N domain are shown (N, orange; D1α/β, light blue; D1α, magenta; D1/D2 linker, pink; D2α/β, blue; D2α, green) in the ATP state. The helix labeling is the same as that used by DeLaBarre & Brunger.[30] (b) Stereo diagram of a close-up view of the area marked by a broken black circle in (a) from the ATP structure. The region shown is the interaction of a loop of the D1α domain with the loop connecting strands β9 and β10 of the N_b domain. A $2F_o - F_c$ phase combined electron density map of the ND1 domain is superimposed on the structure. The electron density map was obtained by phase combination and σ_A weighting; it was computed to 3.2 Å contoured at 1.2 σ (~1.2 $e^-/Å^3$). (c) As (b), but from the ADP structure. The map was computed to 4.25 Å and sharpened by a B_{sharp} factor of -95 $Å^2$.

sensor-2 motif is present in the D1 domain. Unlike the corresponding elements in the D2 domain, the D1 sensor-2 motif remains ordered for all nucleotide states of p97/VCP and Arg359, the residue equivalent to Arg638, interacts with the β-phosphate group of an ADP molecule bound to a neighboring protomer. The interaction in the D1 domain of p97/VCP is similar to the sensor-2 interaction with nucleotide observed in NSF D2 domain, for which there is an interprotomer lysine residue that interacts with the bound nucleotide.[21,26] Interestingly, the AAA domains in NSF have ATPase activities that are opposite to those of the AAA domains in p97/VCP, since it is the D2 domain in NSF that does not actively hydrolyze ATP.[23] We propose that in AAA proteins, arginine or lysine interaction from the sensor-2 loop to a neighboring protomer may be characteristic of invariant structural AAA domains that do not undergo hydrolysis.

Deviations from strict 6-fold symmetry could be observed for the activated states of the p97/VCP (ADP and ATP‡). In particular, the ATP‡ state does not have equivalent occupancy within its D2 nucleotide-binding sites. The asymmetry also manifests itself in different orientations of the various domains, and increases upon loss of the γ-phosphate group: the ADP state shows large asymmetric variations in the position of the N domains. Such an asymmetry is consistent with steady-state kinetic results that show that two protomers cooperate during ATP hydrolysis (unpublished data)[36] and nucleotide-trapping observations that suggest that only two or three protomers will undergo ATP hydrolysis at any one time.[33] The p97/VCP molecule may be priming itself for the large conformational shift that occurs after ADP release, as observed for the GroEl/GroES system.[40] Similar to p97/VCP, the GroEl/GroES ATP‡ structure is nearly identical with the GroEl/GroES ADP structure, but the ADP state has a higher degree of interdomain motion than the ATP‡ state.

One model of protein dislocation by p97/VCP is that the substrate protein does not pass through the central pore, but interacts with the exterior and/or the D2 end of the p97/VCP hexamer. With this model, a complete unfolding of the substrate protein is not necessary, as secondary structure elements in the substrate do not have to be eliminated for passage through the narrow opening at the D1 end of the molecule. The pore opening is only 5.5 Å across in the pre-activated structures and is blocked completely by a zinc ion in both of the activated structures. Furthermore, we observe significant conformational changes on the surface of p97/VCP during the hydrolysis cycle (Figure 3). The alternative model, a through-pore mechanism of substrate processing, would require p97/VCP to unfold proteins completely in order to move them through the central pore. The narrow opening in the D1 end of the pore is probably too tight a fit for unmodified protein substrates and it would provide a significant barrier to the passage of glycosylated substrates. Furthermore, complete unfolding of ERAD substrates after p97/VCP interaction can be accomplished by the proteasome; it is unlikely that such an energy-intensive process would be duplicated within the ERAD pathway.

In summary, we have observed a conformational switch of p97/VCP between pre-activated and activated states, and a transition from a rigid state (as defined by the order of the D1D2 linker and D2α domain) to a flexible state upon loss of the γ-phosphate group, and a further increase in flexibility upon nucleotide release (as defined by the disordering of the D2α domain) (Figures 2 and 3(d)). In addition, the sensor-2 loop undergoes an opposite disorder–order transition upon loss of the γ-phosphate group. These conformational and dynamic changes may provide a driving force for the protein unfolding required during membrane protein extraction or protein dislocation.

We observed significant deviations from 6-fold symmetry for some of the subunits as well as an unequal occupancy of the D2 binding site in the ATP‡ state. The symmetry in p97/VCP may be decreased further by its interactions with adaptor proteins, substrate or membrane. These additional factors may help to impose a directionality on the mechanism of action of p97/VCP and prevent substrate interactions from slipping backwards during dislocation. Assuming multiple hydrolysis cycles, p97/VCP would thus undergo periodic conformational and dynamic changes that could take advantage of random structural fluctuations in the dislocated protein, thereby making incremental interactions with them until they are freed from the membrane.

Materials and Methods

Crystallization

The expression and purification of wild-type and selenomethionine-substituted p97/VCP have been described.[30] For both structures, p97/VCP at a concentration of 14 mg/ml was added in a 1 : 1(v/v) mixture with the crystal growth solution using the hanging-drop, vapor-diffusion method. For the ADP structure, ADP was added to p97/VCP in 30-fold molar excess on the basis of the p97/VCP protomer molecular mass. Diffraction-quality crystals with a paralleliped shape and dimensions of 200 μm×100 μm×100 μm grew within ten days from 100 mM Hepes (pH 7.0 at 21 °C), 5% (w/v) PEG 3350, 50 mM NH_4F, 5 mM DTT. Surprisingly, the selenomethionine-substituted form produced crystals that diffracted to 4.25 Å resolution rather than the ~8 Å resolution typical of the wild-type protein p97/VCP·ADP crystals. Crystals were prepared for cryogenic storage by adding glycerol to a final concentration of 30% (v/v) to the original drop of mother liquor, and then frozen in Hampton crystal loops in liquid nitrogen for subsequent data collection.

For the ATP-state structure, AMP-PNP was added to p97/VCP in 30-fold molar excess on the basis of the p97/VCP protomer molecular mass. Diffraction quality crystals of both the wild-type and selenomethionine

forms, with a hexagonal shape and dimensions of 100 μm×100 μm×100 μm grew within four days from 100 mM sodium citrate buffer (pH 5.0 at 21 °C), 6% (w/v) PEG 400, 0.75 M NaH_2PO_4, 50 mM NH_4F. Conditions for the selenomethionine crystals included 5 mM DTT. Crystals were prepared for cryogenic storage by sequential washing with mother liquor solutions of increasing concentration of glycerol, up to 20% (v/v), and then frozen in a manner similar to that used for the p97/VCP·ADP crystals.

Reprocessing of the diffraction data for the ATP‡ structure

Diffraction data for p97/VCP·ATP‡ crystals were collected as described,[30] but were merged with a data set from the same crystal using increased beam flux and shorter exposures. Radiation damage was evident in the decreased resolution as the data collection progressed, but careful processing resulted in an increase of resolution useful for maximum likelihood refinement from 4.65 Å to 4.4 Å.

Data collection for the ADP structure

The p97/VCP·ADP diffraction data were collected at beamline 8.2.1 of the Advanced Light Source (ALS) at Lawrence Berkeley National Laboratory. The diffraction data were processed with MOSFLM/SCALA (Table 1).[41] Radiation damage prevented the collection of a complete MAD data set to the same resolution visible in initial diffraction images, and so a full three-wavelength MAD data set was collected only at relatively low resolution (Table 1). To minimize radiation damage, the MAD data set was obtained by measuring the inflection and high-energy remote with a standard sweep followed by an inverse beam collection at the peak.[42] A diffraction data set at the selenomethionine absorption peak from a second crystal was collected at a higher resolution, with weak reflections visible beyond 4 Å. The diffraction data collected at the peak wavelength were used for maximum likelihood-based refinement (see below).

Data collection for the ATP structure

For the p97/VCP structure with AMP-PNP, the diffraction data were collected at beamline 11-1 at the Stanford Synchrotron Radiation Laboratory (SSRL). The crystals diffracted anisotropically, to 3.5 Å in the worst direction and 3.1 Å in the best direction. Selenomethionine derivatives suffered from radiation damage during data collection. A complete MAD data set could be collected to a resolution of only ~8 Å. A single-wavelength anomalous dispersion (SAD) data set to 4.5 Å resolution was used as the source of experimental phase information, as inclusion of the low-resolution inflection and remote data sets in this case did not improve phasing statistics or electron density maps.

B-factor sharpening

B-factor sharpening[30,43] of the observed diffraction data produced more side-chain details and improved definition of β-strands and nucleotides in subsequent maps than obtained from un-sharpened maps (for example, see DeLaBarre & Brunger, Figure 1(d)[30]). The B_{sharp} factor was applied to the observed structure factor amplitudes $F(S)$ by:

$$F_{sharp}(S) = \exp(-2B_{sharp}(\sin\theta/\lambda)^{-2})F(S)$$

The optimum value for B_{sharp} was obtained by a modification of the well-known Wilson scaling procedure. Our modified procedure entailed choosing the smallest *B*-value that produced values such that $\langle|F_{sharp}(S)|^2\rangle \geqq \langle f^2\rangle$, where f are the atomic scattering factors of randomly placed atoms with the structure's chemical composition in bin-wise resolution shells. This is an approximation to the assumption of Wilson statistics that the observed structure factors are at least equal to the contribution of the scattering factors of a model of randomly placed atoms. This new approach is an improvement over the previous subjective approach of choosing B_{sharp} values based on inspection of the resulting electron density maps.[30] It should be noted that *B*-factor sharpening was applied only to electron density maps. The original diffraction data were used during for the target function of refinement.

Solution of the ADP structure

The ADP structure was solved by molecular replacement using the previously determined model of the ATP‡ state.[30] The unrefined molecular replacement solution was used to generate phased anomalous difference maps from which the selenomethionine positions were determined. Selenium positions were refined by CNS to obtain experimental phase probability distributions.[44] It was important to iteratively improve the selenium model and experimental phase probability distribution by using the refined model phases as a prior phase probability distribution in order to identify additional scatterers or to improve the parameters of the scatterers. Experimental phase probability distributions for the p97/VCP·ADP selenomethionine MAD and SAD data sets were combined with the phases of the molecular replacement model using σ_A-weighting. The selenomethionine dataset at the peak wavelength was used for subsequent map generation and refinement. The *B*-factor-sharpened phase combined $2F_o - F_c$ electron density maps showed greater detail for the ADP structure than those observed for the ATP‡ structure (see Figure 7(c) for a representative example). Some regions had to be adjusted for out-of-register errors that became apparent when comparing the ADP and ATP‡ electron density maps.

Minor corrections of the ATP‡ structure

Areas of the model where the electron density was ambiguous for the original ATP‡ structure were rebuilt on the basis of the corrected chain trace found in the ADP structure. In addition, a slightly higher-resolution diffraction data set at 4.4 Å resolution (Table 1) was used for the refinement of the ATP‡ structure than the 4.7 Å data set that was used previously.[30] Iterative refinement of the selenium model was used to establish the best possible phases during refinement.

Solution of the ATP structure

The p97/VCP structure with AMP-PNP was solved by molecular replacement with the APO model,[29] which interestingly provided a clearer contrast between correct and incorrect solutions than either the ATP‡ or the ADP models. The positions of the selenomethionine residues in the ND1 domains of the ATP structure were confirmed with phased anomalous difference maps using a SAD data set collected from the selenomethionine derivative of

the protein crystallized under identical conditions. Iterative refinement of the selenium model was used to establish the best possible phases during refinement. However, only one of the methionine positions in the D2 domain of the ATP structure could be identified, all other peaks within the vicinity of the D2 domain were well below the signals observed for the selenium positions in the ND1 domains. The phase combined $2F_o-F_c$ electron density maps of the ATP structure revealed that despite the higher overall resolution, a significant portion of the D2 domain exhibited weak electron density, similar to what was reported for the APO structure.[29] Nevertheless, we were able to trace most of the D2α/β domain of the ATP structure (see below) while most of the D2α domain was disordered. The single selenium position observed in the D2 domain at residue 740 was at a crystal–crystal contact, and was observed in only two of the four protomers in the asymmetric unit.

Modification of the bulk solvent model for refinement

The resolution limit of the diffraction data required a modification of the bulk solvent model used during refinement.[45] This was accomplished in a manner similar to that used for the refinement of the p97/VCP·ATP‡ structure.[30] The PROBE radius and SHRINK value were chosen according to values that produced minimal R_{free} and *R*-values as well as reasonable values for the solvent density (0.1–0.2 $e^{-1}/Å^3$) and solvent *B*-factors (>10 $Å^2$). The PROBE radius and SHRINK value were adjusted as necessary during refinement. The corrections became smaller for models derived from higher-resolution diffraction data and as the respective *B*-factors for individual residues were optimized by refinement (Table 2).

Refinement and map calculations

All map interpretation and model building was performed by simultaneous inspection of density-modified experimental electron density maps and *B*-factor-sharpened, σ_A-weighted phase combined $2F_o-F_c$ maps. Refinement was carried out against unsharpened amplitudes from the diffraction data of the respective native crystal diffraction data and the experimental MAD phase probability distribution, initially using the MLHL and finishing with the MLF target function.[46] The behavior of the R_{free} value during refinement was used to chose the appropriate target. Cross-validation using a 7.5% randomly selected subset of the diffraction data was used to guide the refinement and model building. NCS restraints were used for the protomers during refinement. Separate restraints were applied to each of the main domains and linker regions. The restraints were relaxed or removed for regions that consistently refined to unique conformations. In contrast to the original ATP‡ structure,[30] no secondary structure restraints were applied, since the improved resolution of the diffraction data and corrected chain trace produced a stable refinement in the absence of such restraints. Atomic *B*-factors were refined by groups defined by individual residues, with side-chain and main chain defined as two separate groups. The refinement was restrained such that the main-chain atoms had lower *B*-values than their side-chain atoms. The nucleotides were positioned manually into *B*-sharpened $2F_o-F_c$, σ_A-weighted phase-combined electron density and then allowed to be refined independently. All phasing and refinement calculations were performed with CNS;[44] model building was carried out with O;[47] and all molecular images were generated by Pymol,[48] except for Figure 1, which was created with POVSCRIPT+.[49]

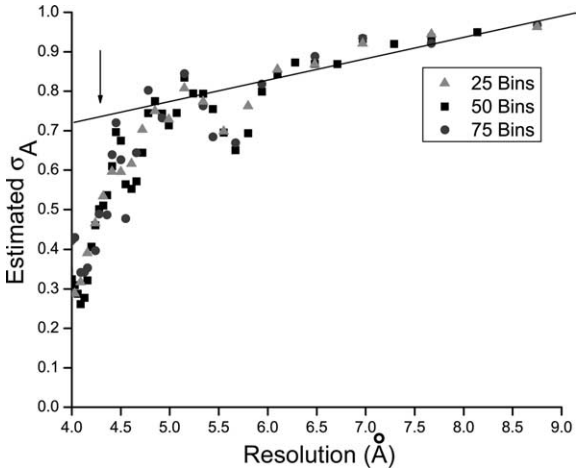

Figure 8. Plot of σ_A *versus* resolution for the ADP dataset. The cross-validated σ_A value for the ADP structure is plotted *versus* resolution. The subset of the diffraction data used for the calculation of the free *R* value was used for computation of σ_A. The continuous line was obtained by linear fit to the diffraction data, and the arrow at 4.25 Å indicates the resolution at which σ_A drops sharply from its previous value. This was taken as the effective limit of the diffraction data useful for structure refinement.[50] The estimated σ_A value was essentially invariant when using 25, 50 or 75 total bins for calculation of σ_A.

Effective resolution limit for the structures

The effective resolution of the refinements (Table 2) was determined by using the behavior of σ_A as a guide (Figure 8).[50] There are many significant (i.e. clearly visible) reflections past the conventional cutoff $I/\sigma_I>3$ cutoff that would otherwise have been omitted from the data analysis. Noisy or weak reflections are automatically down-weighted in the likelihood-based target function.

All visible reflections were used in difference electron density map calculations for rebuilding stages during refinement. A few reflections for both ADP and p97/VCP·ATP‡ crystals were observed to $d_{min}=3.8$ Å.

Final models

The final model refinement statistics are shown in Table 2. The following residues are missing or their side-chains are set to zero occupancy due to weak electron density: for the ATP structure, residues 1–26, 504–505, 568–574, 634–637, and 764–806 in all three independent protomers; for the ADP structure, residues in each of the three independent protomers (A, B, and C): 1–26, 505–506, 567–571, 588–597, 634–637, and 759–806; for the ATP structure, residues 1–16, 469–482, 496–505, and 743–806 in all protomers A–D, and residues 737–743 for the B and D protomers. Note that the missing residues comprise most of the D2α domain for the ATP structure.

Quantification of conformational variability: deviation from 6-fold symmetry

The three independent protomers (A, B, and C) were aligned by their respective invariant D1 α/β domains for both the ATP and ATP‡ structures. Distance vectors between corresponding C^{α} atoms in the three protomers were converted to anisotropic tensors and displayed as pseudo-thermal ellipsoids,[49] colored according to the degree of the root-mean-square difference (r.m.s.d.) of the distances.

Quantification of nucleotide-dependent conformational changes

The domains were defined as follows: N domain, residues 34–186; D1α/β domain, residues 224–357; D1α domain, residues 382–453; D2α/β domain, residues 480–633. The demarcation and rigid-body nature of these domains was established with the program DYNDOM.[51] The D2α domain was omitted from the analysis because of poor definition in the ATP and APO structures. The D1α/β domain was chosen as a reference point for domain motion because it showed only minimal variance after the application of 30°, 60° and 120° rotations about the central axis of the hexamer. All domain changes were determined with LSQMAN,[52] by first aligning the D1α/β domains of the protomers being examined, and then performing an alignment of the domain in question. The rotational angle equivalent to the κ angle from the rotation matrix was used as a measure of domain rotation.

PDB accession codes

The coordinates and structure factors have been deposited in the RCSB Protein Data Bank with accession codes 1YQO, 1YQI and 1YPW.

Acknowledgements

We thank Tim Fenn for assistance with calculating and rendering the pseudo-anisotropic *B*-factors, Tim Fenn and Piet Gros for a critical reading of the manuscript, and the staff members of the Advanced Light Source (ALS) and the Stanford Synchrotron Radiation Laboratory (SSRL) for assistance during data collection. Portions of this research were carried out at the SSRL, a national user facility operated by Stanford University on behalf of the US Department of Energy, Office of Basic Energy Sciences. The SSRL Structural Molecular Biology Program is supported by the Department of Energy, Office of Biological and Environmental Research, and by the National Institutes of Health, National Center for Research Resources, Biomedical Technology Program, and the National Institute of General Medical Sciences. Portions of this research were conducted at AlS, which is supported by the Director, Office of Science, Office of Energy Research, Office of Basic Energy Sciences, Materials Sciences Division, of the US Department of Energy under contract no. DE-AC03-76SF00098 at Lawrence Berkeley National Laboratory.

References

1. Wang, Q., Song, C. C. & Li, C. C. H. (2004). Molecular perspectives on p97-VCP: progress in understanding its structure and diverse biological functions. *J. Struct. Biol.* **146**, 44–57.
2. Pinter, M., Jekely, G., Szepesi, R. J., Farkas, A., Theopold, U., Meyer, H. E. *et al*. (1998). TER94, a Drosophila homolog of the membrane fusion protein CDC48/p97, is accumulated in nonproliferating cells: in the reproductive organs and in the brain of the imago. *Insect. Biochem. Mol. Biol.* **28**, 91–98.
3. Frohlich, K. U., Fries, H. W., Rudiger, M., Erdmann, R., Botstein, D. & Mecke, D. (1991). Yeast cell cycle protein CDC48p shows full-length homology to the mammalian protein VCP and is a member of a protein family involved in secretion, peroxisome formation, and gene expression. *J. Cell. Biol.* **114**, 443–453.
4. Feiler, H. S., Desprez, T., Santoni, V., Kronenberger, J., Caboche, M. & Traas, J. (1995). The higher plant *Arabidopsis thaliana* encodes a functional CDC48 homologue which is highly expressed in dividing and expanding cells. *EMBO J.* **14**, 5626–5637.
5. Roggy, J. L. & Bangs, J. D. (1999). Molecular cloning and biochemical characterization of a VCP homolog in African trypanosomes. *Mol. Biochem. Parasitol.* **98**, 1–15.
6. Ye, Y., Meyer, H. H. & Rapoport, T. A. (2001). The AAA ATPase Cdc48/p97 and its partners transport proteins from the ER into the cytosol. *Nature*, **414**, 652–656.
7. Jarosch, E., Taxis, C., Volkwein, C., Bordallo, J., Finley, D., Wolf, D. H. & Sommer, T. (2002). Protein dislocation from the ER requires polyubiquitination and the AAA-ATPase Cdc48. *Nature Cell Biol.* **4**, 134–139.
8. Rabinovich, E., Kerem, A., Frohlich, K. U., Diamant, N. & Bar-Nun, S. (2002). AAA-ATPase p97/Cdc48p, a cytosolic chaperone required for endoplasmic reticulum-associated protein degradation. *Mol. Cell. Biol.* **22**, 626–634.
9. Kozutsumi, Y., Segal, M., Normington, K., Gething, M. J. & Sambrook, J. (1988). The presence of malfolded proteins in the endoplasmic reticulum signals the induction of glucose-regulated proteins. *Nature*, **332**, 462–464.
10. Asai, T., Tomita, Y., Nakatsuka, S., Hoshida, Y., Myoui, A., Yoshikawa, H. & Aozasa, K. (2002). VCP (p97) regulates NFkappaB signaling pathway, which is important for metastasis of osteosarcoma cell line. *Jpn. J. Cancer Res.* **93**, 296–304.
11. Dai, R. M. & Li, C. C. (2001). Valosin-containing protein is a multi-ubiquitin chain-targeting factor required in ubiquitin-proteasome degradation. *Nature Cell Biol.* **3**, 740–744.
12. Rape, M., Hoppe, T., Gorr, I., Kalocay, M., Richly, H. & Jentsch, S. (2001). Mobilization of processed, membrane-tethered SPT23 transcription factor by CDC48(UFD1/NPL4), a ubiquitin-selective chaperone. *Cell*, **107**, 667–677.
13. Meyer, H. H., Shorter, J. G., Seemann, J., Pappin, D. & Warren, G. (2000). A complex of mammalian ufd1 and npl4 links the AAA-ATPase, p97, to ubiquitin and nuclear transport pathways. *EMBO J.* **19**, 2181–2192.
14. Meyer, H. H., Kondo, H. & Warren, G. (1998). The p47 co-factor regulates the ATPase activity of the membrane fusion protein, p97. *FEBS Letters*, **437**, 255–257.
15. Ye, Y., Meyer, H. H. & Rapoport, T. A. (2003). Function of the p97-Ufd1-Npl4 complex in retrotranslocation

from the ER to the cytosol: dual recognition of nonubiquitinated polypeptide segments and polyubiquitin chains. *J. Cell Biol.* **162**, 71–84.
16. Hetzer, M., Meyer, H. H., Walther, T. C., Bilbao-Cortes, D., Warren, G. & Mattaj, I. W. (2001). Distinct AAA-ATPase p97 complexes function in discrete steps of nuclear assembly. *Nature Cell Biol.* **3**, 1086–1091.
17. Ye, Y. H., Shibata, Y., Yun, C., Ron, D. & Rapoport, T. A. (2004). A membrane protein complex mediates retro-translocation from the ER lumen into the cytosol. *Nature*, **429**, 841–847.
18. Lilley, B. N. & Ploegh, H. L. (2004). A membrane protein required for dislocation of misfolded proteins from the ER. *Nature*, **429**, 834–840.
19. Babor, S. M. & Fass, D. (1999). Crystal structure of the Sec18p N-terminal domain. *Proc. Natl Acad. Sci. USA*, **96**, 14759–14764.
20. May, A. P., Misura, K. M., Whiteheart, S. W. & Weis, W. I. (1999). Crystal structure of the amino-terminal domain of N-ethylmaleimide-sensitive fusion protein. *Nature Cell Biol.* **1**, 175–182.
21. Yu, R. C., Hanson, P. I., Jahn, R. & Brunger, A. T. (1998). Structure of the ATP-dependent oligomerization domain of N-ethylmaleimide sensitive factor complexed with ATP. *Nature Struct. Biol.* **5**, 803–811.
22. Coles, M., Diercks, T., Liermann, J., Groger, A., Rockel, B., Baumeister, W. *et al*. (1999). The solution structure of VAT-N reveals a 'missing link' in the evolution of complex enzymes from a simple betaalphabetabeta element. *Curr. Biol.* **9**, 1158–1168.
23. Brunger, A. T. & DeLaBarre, B. (2003). NSF and p97/VCP: similar at first, different at last. *FEBS Letters*, **555**, 126–133.
24. Dalal, S., Rosser, M. F., Cyr, D. M. & Hanson, P. I. (2004). Distinct roles for the AAA ATPases NSF and p97 in the secretory pathway. *Mol. Biol. Cell*, **15**, 637–648.
25. Neuwald, A. F., Aravind, L., Spouge, J. L. & Koonin, E. V. (1999). AAA+: A class of chaperone-like ATPases associated with the assembly, operation, and disassembly of protein complexes. *Genome Res.* **9**, 27–43.
26. Lenzen, C. U., Steinmann, D., Whiteheart, S. W. & Weis, W. I. (1998). Crystal structure of the hexamerization domain of N-ethylmaleimide-sensitive fusion protein. *Cell*, **94**, 525–536.
27. Hattendorf, D. A. & Lindquist, S. L. (2002). Analysis of the AAA sensor-2 motif in the C-terminal ATPase domain of Hsp104 with a site-specific fluorescent probe of nucleotide binding. *Proc. Natl Acad. Sci. USA*, **99**, 2732–2737.
28. Bowman, G. D., O'Donnell, M. & Kuriyan, J. (2004). Structural analysis of a eukaryotic sliding DNA clamp-clamp loader complex. *Nature*, **429**, 724–730.
29. Huyton, T., Pye, V. E., Briggs, L. C., Flynn, T. C., Beuron, F., Kondo, H. *et al*. (2003). The crystal structure of murine p97/VCP at 3.6 Å. *J. Struct. Biol.* **144**, 337–348.
30. DeLaBarre, B. & Brunger, A. T. (2003). Complete structure of p97/Valosin-containing protein reveals communication between nucleotide domains. *Nature Struct. Biol.* **10**, 856–863.
31. Zhang, X., Shaw, A., Bates, P. A., Newman, R. H., Gowen, B., Orlova, E. *et al*. (2000). Structure of the AAA ATPase p97. *Mol. Cell.* **6**, 1473–1484.
32. Rouiller, I., DeLaBarre, B., May, A. P., Weis, W. I., Brunger, A. T., Milligan, R. A. & Wilson-Kubalek, E. M. (2002). Conformational changes of the multifunction p97 AAA ATPase during its ATPase cycle. *Nature Struct. Biol.* **9**, 950–957.
33. Zalk, R. & Shoshan-Barmatz, V. (2003). ATP-binding sites in brain p97/VCP (valosin-containing protein), a multifunctional AAA ATPase. *Biochem. J.* **374**, 473–480.
34. Wang, Q., Song, C. & Li, C. C. (2003). Hexamerization of p97-VCP is promoted by ATP binding to the D1 domain and required for ATPase and biological activities. *Biochem. Biophys. Res. Commun.* **300**, 253–260.
35. Wang, Q., Song, C., Yang, X. & Li, C. C. (2003). D1 ring is stable and nucleotide-independent while D2 ring undergoes major conformational changes during the ATPase cycle of p97-VCP. *J. Biol. Chem.* **13**, 13.
36. Song, C., Wang, Q. & Li, C. C. (2003). ATPase activity of p97-valosin-containing protein (VCP), D2 mediates the major enzyme activity, and D1 contributes to the heat-induced activity. *J. Biol. Chem.* **278**, 3648–3655.
37. Watts, G. D., Wymer, J., Kovach, M. J., Mehta, S. G., Mumm, S., Darvish, D. *et al*. (2004). Inclusion body myopathy associated with Paget disease of bone and frontotemporal dementia is caused by mutant valosin-containing protein. *Nature Genet.* **36**, 377–381.
38. Dreveny, I., Kondo, H., Uchiyama, K., Shaw, A., Zhang, X. & Freemont, P. S. (2004). Structural basis of the interaction between the AAA ATPase p97/VCP and its adaptor protein p47. *EMBO J.* **23**, 1030–1039.
39. Beyer, A. (1997). Sequence analysis of the AAA protein family. *Protein Sci.* **6**, 2043–2058.
40. Chaudhry, C., Horwich, A. L., Brunger, A. T. & Adams, P. D. (2004). Exploring the structural dynamics of the *E. coli* chaperonin GroEL using translation-libration-screw crystallographic refinement of intermediate states. *J. Mol. Biol.* **342**, 229–245.
41. Collaborative Computational Project, Number 4. (1994). The CCP4 suite: programs for protein crystallography. *Acta Crystallog. sect. D*, **50**, 760–763.
42. Gonzalez, A. (2003). Optimizing data collection for structure determination. *Acta Crystallog. sect. D*, **59**, 1935–1942.
43. Bass, R. B., Strop, P., Barclay, M. & Rees, D. C. (2002). Crystal structure of *Escherichia coli* MscS, a voltage-modulated and mechanosensitive channel. *Science*, **298**, 1582–1587.
44. Brunger, A. T., Adams, P. D., Clore, G. M., DeLano, W. L., Gros, P., Grosse-Kunstleve, R. W. *et al*. (1998). Crystallography & NMR system: a new software suite for macromolecular structure determination. *Acta Crystallog. sect. D*, **54**, 905–921.
45. Jiang, J. S. & Brunger, A. T. (1994). Protein hydration observed by X-ray diffraction. Solvation properties of penicillopepsin and neuraminidase crystal structures. *J. Mol. Biol.* **243**, 100–115.
46. Pannu, N. S., Murshudov, G. N., Dodson, E. J. & Read, R. J. (1998). Incorporation of prior phase information strengthens maximum-likelihood structure refinement. *Acta Crystallog. sect. D*, **54**, 1285–1294.
47. Jones, T. A., Zou, J. Y., Cowan, S. W. & Kjeldgaard (1991). Improved methods for building protein models in electron density maps and the location of errors in these models. *Acta Crystallog. sect. A*, **47**, 110–119.
48. DeLano, W. L. (2002). *The PyMol User's Manual*, DeLano Scientific, San Carlos, CA.
49. Fenn, T. D., Ringe, D. & Petsko, G. A. (2003).

POVScript+: a program for model and data visualization using persistence of vision ray-tracing. *J. Appl. Crystallog.* **36**, 944–947.
50. Ling, H., Boodhoo, A., Hazes, B., Cummings, M. D., Armstrong, G. D., Brunton, J. L. & Read, R. J. (1998). Structure of the shiga-like toxin I B-pentamer complexed with an analogue of its receptor Gb3. *Biochemistry*, **37**, 1777–1788.
51. Hayward, S. & Berendsen, H. J. (1998). Systematic analysis of domain motions in proteins from conformational change: new results on citrate synthase and T4 lysozyme. *Proteins: Struct. Funct. Genet.* **30**, 144–154.
52. Kleywegt, G. J. (1996). Use of Non-crystallographic Symmetry in Protein Structure Refinement. *Acta Crystallog. sect. D*, **52**, 842–857.
53. Morris, A. L., MacArthur, M. W., Hutchinson, E. G. & Thornton, J. M. (1992). Stereochemical quality of protein structure coordinates. *Proteins: Struct. Funct. Genet.* **12**, 345–364.

Edited by R. Huber

(Received 7 December 2004; received in revised form 18 January 2005; accepted 21 January 2005)